

Application of the arctangent function model in the prediction of ground mining subsidence deformation: a case study from Fushun City, Liaoning Province, China

Lei Nie¹ · Hongfei Wang¹ · Yan Xu¹

Received: 4 March 2016 / Accepted: 23 June 2016 / Published online: 6 July 2016
© Springer-Verlag Berlin Heidelberg 2016

Abstract Ground subsidence disasters are characterized by wide distribution, long duration, and high-intensity damage, which can cause serious damages to surface buildings, underground pipelines, aquifers, and so on. Therefore, research on the stability evaluation of ground subsidence and subsidence deformation prediction is of great significance. This paper takes ground subsidence in Fushun City, Liaoning Province, China, as a case study. Combined with data from 60 monitoring points in the subsidence areas, the final settlement deformation values of all monitoring points were obtained through an arctangent function model using non-linear curve fitting with monitoring data. The proposed model could enable the prediction of settlement deformation trends of the monitoring points. Correlation coefficients are all above 0.937, indicating the strong reliability of the prediction model. By processing the final settlement deformation predictive values of the 60 monitoring points, a final settlement contour map was drawn with the help of the Kriging interpolation method. This map could forecast the whole distribution characteristics of ground settlement deformation in the research area. Then, risk zoning can be obtained by combining the settlement rate and residual settlement deformation in the study area. The research results could provide a basis for future city construction and regional planning in Fushun City.

Keywords Ground subsidence · Deformation prediction · Arctangent function model · Non-linear curve fitting · Kriging interpolation method · Risk zoning

Introduction

Owing to the long history of mining, ground subsidence disasters occur frequently, bringing serious damages to the buildings located throughout mining cities. Such ground subsidence hazards threaten the industries, ultimately affecting the economic development of mining cities. Thus, studying the distribution characteristics and finding prediction models to determine ground subsidence deformation are important research topics.

Geological hazards due to ground subsidence are a common problem in the production and construction industries around the world. Research on such geological hazards caused by underground mining is also an important topic among researchers all over the world. Lei et al. (2013) conducted numerical simulations of ground subsidence caused by coal mining to study the surface collapse mechanism and regularity. Sheorey et al. (2000) used a modified influence function method to complete subsidence prediction. Gonzalez-Nicieza et al. (2007) researched the influence of time on subsidence. Cui et al. (2001) used a time function to predict the progressive surface subsidence above long-wall coal mining using a time function. Ruisheng et al. (2011) proposed a 3D stratigraphic model that mixed Multi-DEM with a tetrahedral network model. Their 3D stratigraphic model is an accurate prediction model that can provide detailed data on geological mining conditions for mining subsidence prediction research. Zhang Bin et al. (2015) researched subsidence prediction and susceptibility zonation for collapse above

✉ Hongfei Wang
whf001988@126.com

¹ College of Construction Engineering, Jilin University, Changchun 130026, People's Republic of China

goaf with thick alluvial cover. In order to solve the uncertainty of the influence factors of mining subsidence and the difficulty of obtaining prediction model parameters, Huaifeng et al. (2014) used the grey prediction model to forecast ground subsidence. Cui et al. (2013) conducted the prediction work of ground subsidence due to underground mining based on the zenith angle. Zhanqiang et al. (2015) introduced a novel ground subsidence prediction model for sub-critical mining in studying the geological condition of a thick alluvium layer. The different subsidence and displacement mechanisms for the rock mass and the thick alluvium layers are respectively considered and described in this model. Díaz-Fernández et al. (2010) presented a computer tool that automatically predicts mining subsidence using the generalized n - k - g influence function. The n - k - g influence function depends on two physical concepts: the first is gravity, which characterizes the forces acting on the ground, and the second, the convergence of the roof and floor of the mine workings due to the stress state of the ground.

Consistent surface monitoring in Fushun City has generated rich real-time monitoring data to facilitate research on mining subsidence deformation. Nie et al. (2015) proposed a new prediction model for mining subsidence deformation: the arctangent function model according to the “S” type settlement curve of monitoring point G22. G22 is a GPS leveling measurement point at the Taihe Coal Mine, and the position is shown in Fig. 2. They used the model to investigate a collapsed pit in the Taihe coal mine in Fushun, Liaoning Province, China, and the area’s mining subsidence deformation characteristics. Their model capably predicted the final settlement deformation value of the G22 monitoring point. Despite the above-mentioned studies, further research on the overall distribution regularity and prediction of ground settlement deformation and the risk zoning in the mining area has yet to be conducted.

The current paper takes the ground subsidence phenomenon in Fushun, Liaoning Province, China, as the case study. Combined with data from 60 monitoring points in the study area, the model parameters are obtained through the arctangent function model nonlinear curve fitting with the monitoring data. The asymptote value of the “S” type arc tangent function is the final settlement deformation value of the monitoring points, and then the prediction of a subsidence deformation trend of the monitoring points are realized. The residual subsidence deformation values from now to the final settlement stability are obtained by combining the current accumulation subsidence deformation values with the predicted final subsidence deformation values. Finally, the current ground settling velocity is identified by using the mathematical properties of the arctangent function. By processing the final subsidence deformation values, the residual subsidence deformation

values, and the current ground settling velocity values of the 60 monitoring points with the help of the Kriging interpolation method, the corresponding contour maps are drawn. The contour maps display the overall distribution characteristics of ground settlement deformation in the study area and predict the development trend.

Finally, the risk zoning of the study area is put forward by combining the distribution characteristics of the current settling velocity and the residual subsidence deformation. The data are used to determine the stable region and the different danger levels of the unstable regions. Such information could be used as basis for city construction and regional planning in Fushun.

Study area and monitoring data

Geographical location and the present situation of ground subsidence disaster in the study area

Fushun city is located in the east part of Liaoning Province, 48 km to Shenyang (Fig. 1). The geographical coordinates lie roughly at a longitude of 123°39′ to 125°28′ and a latitude of 41°38′ to 42°14′. The urban area is 713.6 km². The city’s total population is 2.25 million people, including the urban population of 1.42 million people.

Fushun City is famous for its mining industry, and its coal mines have been exploited since 1901. Ground subsidence hazards caused by nearly 100 years of underground coal mining have brought the city increasingly serious environmental and economic problems. Variations in the ground elevation of the local area occurred in a short period of time, which caused serious damage to buildings, underground pipelines, road, bridges, and dams. The

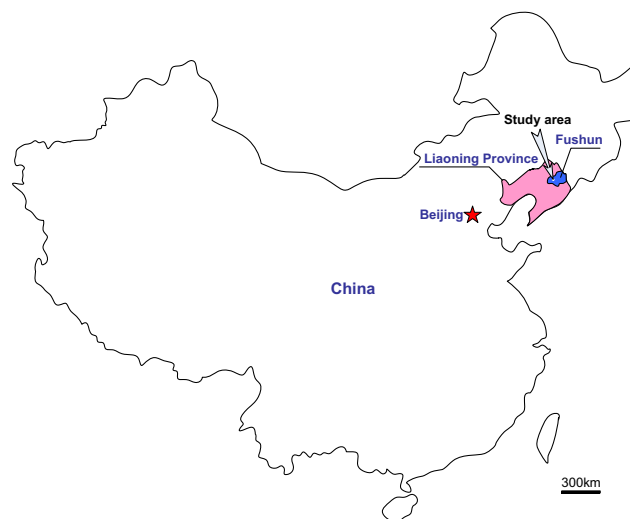


Fig. 1 Location of the study area (Nie et al. 2015)

continuous sinking of grounds in urban and industrial areas also endanger the lives and properties of the inhabitants.

Ground subsidence in Fushun City is characterized by wide distribution, long duration, and high-intensity damage. If the distribution characteristics and development trends of ground settlement deformation are not clear, these could be a major factor in destabilizing the harmonious and sustainable development of Fushun City and its economy. Therefore, further development of Fushun ground subsidence prediction, from which the distribution characteristics and development trends of ground settlement deformation in the mining areas could be obtained, is of great significance to public safety and the sustainable development of the economy.

General situation of mining areas in the study area

The study area in this paper mainly spans the southern portion of the Hun He River and the northern area of the east open-pit mine, which includes the east open-pit mining area as well as Longfeng, Laohutai, and Taihe coal mining areas, covering an area of 27.7 km² (Fig. 2). The profile of the study area is shown in Fig. 3, and its location is in the Laohutai mine area as shown in Fig. 2.

The east open-pit mine is 6.0 km long from west to east and 1.5 km wide from north to south, covering an area of 9.0 km². The main productions are residual coal and oil shale in the Longfeng and Laohutai mines. By the end of 2000, there were 82.85 Mt of coal reserves and 7.48×10^3 Mt of oil shale ores (oil content of more than 4.7 %) in the east open-pit. The east open-pit mine is at the normal mining stage, but has not yet reached the scale.

The Laohutai mine, which has an area of about 10.0 km², is in the bottom of the east open-pit. Mining started here in 1901. Before the founding of the People's Republic in 1949, the mine had already produced 0.33×10^3 Mt of coal. Until 2001, the cumulative coal

production was 1.77×10^3 Mt. From 2001 to 2004, raw coal production was 12.70 Mt. As of late 2004, the Laohutai field has been reported to have reserves of 55.60 Mt, which contains 28.40 Mt residual coal from the Longfeng mine. The Laohutai ore mining mechanization degree is 100 %. A recovery method of over -580 m from sea level is intended for blast mining and longwall caving. Overburden failure is an important factor in safety assessments in the fields of mining engineering geology and safety geology (Wanghua et al. 2015). Mining at -730 m from sea level has been done, and -830 m from sea level is being planned.

The Longfeng mine is located in the eastern part of the study area; it is 5.0 km long from east to west, 2.5 km wide between north and south, and covers an area of 12.5 km² (including Taihe). Operations here began in 1907 and ended in the latter part of 1999. The cumulative coal quantity of the Longfeng coal mine is 1.41×10^3 Mt. The subsidence area in the Longfeng coal mine is 8.12 km². The mine closed in 1999 due to bankruptcy. Once mining operations stopped, the ground was reported to be at the stage of residual subsidence deformation, wherein deformation is small and the ground tends to be on a nearly stable state.

The Taihe coal mine was established in 2000. The mining area, which is about 1.93 km², is located in the southwest corner of the Longfeng mine. By the end of 2008, the mine coal reserves were 13.40 Mt. The mining elevation of the Taihe coal mining is -440 to -530 m from sea level, and the caving mining method is used here.

Monitoring data and ground subsidence in the study area

The high frequency of surface subsidence after 2010 drew the attention of the government. Geodetic monitoring is an effective tool to study ground subsidence deformation

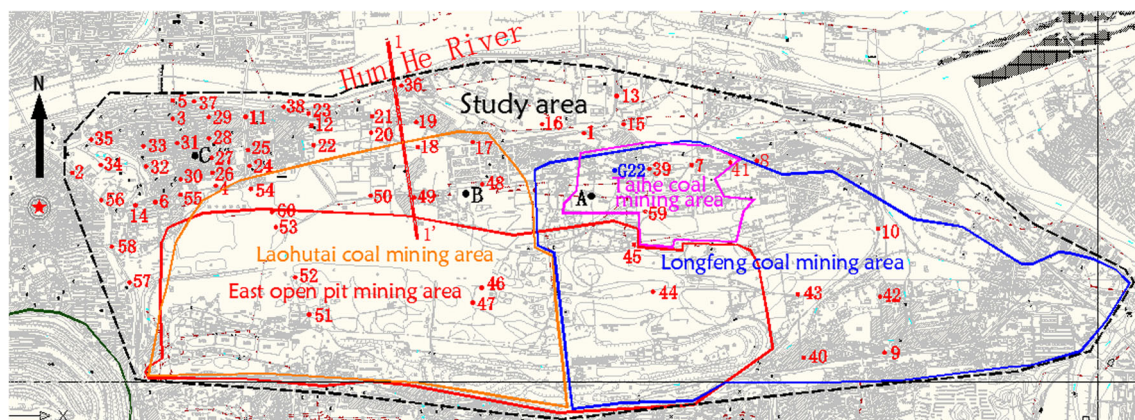


Fig. 2 Distribution map of the mining areas and the monitoring points

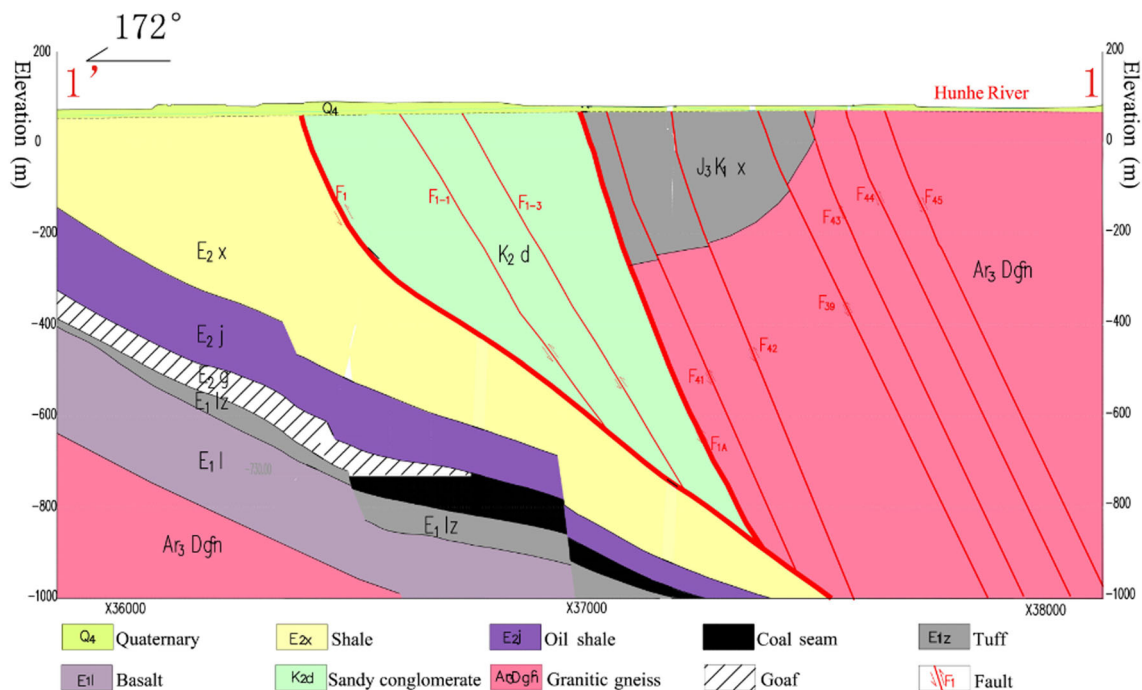


Fig. 3 Profile of the study area

characteristics (David Lamich et al. 2015). In order to understand the distribution and regularity of the ground subsidence deformation in the mine, 60 real-time kinematic (RTK) GPS monitoring points were set up to monitor ground subsidence deformation in the study area. The locations of the monitoring points are shown in Fig. 2. The monitoring data from the 1st to 18th points are shown in Table 1, those from the 19th to 38th points are shown in Table 2, and those of the 39th to 60th points are shown in Table 3. The initial monitoring time of the 60 monitoring points is unified in the paper, corresponding to the date of September 23, 2010. Due to the different location of monitoring points, the time effect of the stress–strain transfer in the spatial medium will lead to the lag of the subsidence deformation of the individual monitoring points that are far away from the mining area. Model fitting requires the use of effective data after the subsidence begins, so invalid data in Tables 1, 2, and 3 were omitted, and only the data after the start of settlement deformation are displayed. The initial monitoring time may not be the starting time of the settlement, so the cumulative settlement value of 0 is set initially, and is not the real cumulative value since the beginning of ground settlement. The cumulative settlement values and monitoring times from the day corresponding to 0 settlement value are then collected. The most effective monitoring time was from September 23, 2010, to May 15, 2013. In Table 4, for the monitoring points of which the starting time of the settlement is later than the initial monitoring time, the date

corresponding to a 0 settlement value is defined as the initial monitoring time and the starting time of the settlement.

The 46th, 47th, 51th, 52th, 53th, and 60th monitoring points are located in the east open-pit mining area, however, their final accumulated subsidence monitoring values are not large. This phenomenon may be related to the location of the monitoring points on a relatively stable mining operation platform. In addition, the main ore mining area in the neighboring Laohutai mine in the north has little impact on the former.

The 17th, 18th, 48th, 54th, 49th, and 50th monitoring points are located in the Laohutai mining area. Their final settlement deformation values are relatively bigger, except for that of the 48th monitoring point. The monitoring results are in line with the region's severe ground subsidence phenomenon, as shown in Fig. 4c. The ground surface crack caused by uneven settlement is related to a large degree of underground mining in the Laohutai coal mine and the accelerating stage of “S” type subsidence deformation in the area.

The 9th, 10th, 40th, 42th, 43th, 44th, and 45th monitoring points are located in the Longfeng mining area. The final monitoring settlement values are generally small, and the ground survey also shows that the regional ground subsidence phenomenon is not significant.

The 7th, 39th, 41th, and 59th monitoring points are located in the Taihe mining area. From the final monitoring values, it can be seen that ground subsidence phenomenon

Table 1 Monitoring data from the 1st to 18th monitoring points

Date (year/month/day)	1	2	3	4	5	6	7	8	9	10	11	12	13	14	15	16	17	18	
2010/9/23												0.00	0.00	0.00	0.00	0.00	0.00	0.00	0.00
2010/11/9												0.07		0.77		2.33		2.69	0.19
2010/12/28								0.00	0.00	0.00	0.00	0.12	2.42	16.20	0.12		7.80		5.67
2011/2/23							0.00	0.80	0.78	0.08	0.23	0.91	3.48		1.24				13.43
2011/4/20							7.34	0.81	1.30	0.32	1.27	4.19	4.48	16.71	3.41	5.08	32.59		13.51
2011/6/21						0.00	11.47	0.83	1.77	0.35	7.35		17.92	21.50	4.63	6.00			
2011/7/19		0.00				1.07	18.58	1.50	2.01	0.51	8.17		21.13	24.80	19.18	8.06			
2011/9/5		0.57	0.00	0.00	0.21	1.08	19.57		2.56	0.60	25.23		25.90	25.59	21.23	8.16	72.20		
2011/10/4		1.87	0.61	0.63	0.23	3.62	27.11		3.42	0.80	25.68		25.95	25.92	23.38	8.65	72.20		
2011/10/26		1.88	0.64	0.68	0.35	3.82	47.35	1.60	3.83	0.80	26.77		26.99	26.82	24.75	9.27	72.83		
2011/11/17		1.94	1.71	1.39	0.46	4.81	58.26	1.67	5.31	0.94	26.89		27.46	27.81	25.41	9.56	73.21		
2011/12/8		2.01	1.72	2.85	0.55	5.03	63.43	1.77	5.65	1.10	26.92		27.65	28.37	28.66	10.16	73.18		
2011/12/29		4.82	1.46	3.13	0.63	5.37	71.17	1.81	6.92	1.12	27.40		27.98	28.99	33.93	10.65	74.51		
2012/1/20		6.13	2.78	4.06	0.67	5.70	74.70	2.18	7.89	1.21	27.62		29.05	29.07	34.02	10.73	74.89		
2012/2/15		7.62	4.45	4.12	0.88	5.77	79.11	2.30	8.25	1.50	27.73		30.77	29.42	35.54	12.49	74.90		
2012/3/18		7.93	6.07	4.27	1.23	6.32	85.07	3.28	8.96	1.65	27.80		30.84	29.91	37.66	12.58	75.92		
2012/4/10			8.33	4.64	1.32	7.39	89.52	3.33	8.97	1.71	29.18		32.40	30.66	37.75	12.83	75.93	72.85	
2012/5/5			10.41	5.53	1.41	7.52	93.84	3.48	10.83	1.82	35.24		32.90	30.86	39.97	13.38	75.98	79.36	
2012/5/21			11.29	9.07	1.70	7.85	96.06	4.14	11.08	2.48	36.65		33.15	31.64	39.59	14.82	76.20	80.86	
2012/6/20			12.41	9.66	1.83	8.30	99.64	4.34	11.40	2.63	39.71		33.19	31.69	40.29	17.14	76.80	93.87	
2012/7/2			19.64	9.75	1.90	8.58	99.71	5.16	11.64	3.09	41.01	18.03	34.11	33.92	41.16	17.39	78.66	98.71	
2012/7/16		0.00		27.02	10.38	2.23	9.17	107.53	5.47	11.79	3.12	42.59	34.31	35.09	41.72	17.40	80.16	103.30	
2012/8/10		0.77		29.55	13.73	2.24	9.26	107.82	5.62	11.99	3.27	46.42	33.77	37.53	42.13	20.02	81.27	107.67	
2012/9/3		16.23		29.10	19.78	2.26	10.62	110.24	6.76	12.68	3.28	47.75	36.14	37.80	43.91	20.78	83.22		
2013/1/19		109.78											37.58		45.24	22.46			
2013/2/22		107.73					113.55	7.95											
2013/4/28		121.58		31.46	36.63	2.34	10.67	127.41	8.75	13.04	5.15	53.32						91.86	
2013/5/15		128.41		30.90		3.02	11.55	132.84	11.54	19.63	9.12	52.62	39.87		49.31			90.52	

Table 2 Monitoring data from the 19th to 38th monitoring points

Date (year/month/day)	The cumulative settlement deformation δ /mm																														
	19	20	21	22	23	24	25	26	27	28	29	30	31	32	33	34	35	36	37	38											
2010/9/23	0.00	0.00	0.00	0.00	0.00	0.00	0.00	0.00	0.00	0.00	0.00	0.00	0.00	0.00	0.00	0.00	0.00	0.00	0.00	0.00	0.00	0.00	0.00	0.00	0.00	0.00	0.00	0.00	0.00		
2010/11/9	0.12	1.92	3.06	5.65	0.43	0.39	0.86	0.04	5.72	3.58	0.03	1.49	0.96	0.29	0.30														1.26		
2010/12/28	0.56	3.06	3.20	8.15	5.11	2.20	1.05																						1.15		
2011/2/23	0.70			8.66	2.37	4.01								0.69															3.48		
2011/4/20	0.75			14.43	17.28	3.26	4.35	6.14						0.84																	
2011/6/21	1.05			18.24	0.00	1.69	16.98	10.49						1.87													2.04	2.45			
2011/7/19	1.70			18.32	4.52	41.69	12.09	3.82					4.24													0.77	1.39	0.00	2.07	2.46	4.38
2011/9/5	1.89			65.08	18.54	5.48	43.39	13.62	4.10	0.67			7.67	1.58	9.90	1.64										9.90	1.64	2.31	4.33	4.40	
2011/10/4	2.29	2.31	3.50	65.27	19.16	7.08	50.33	13.79	5.31				7.78	1.84	10.45	2.45	1.41									10.45	2.45	2.51	3.46	5.01	
2011/10/26	2.45	5.04	5.04	63.64	19.86	10.33	50.53	13.83	5.59	0.91			8.46	2.20	11.50	2.79	1.76									11.50	2.79	2.61	4.44	5.06	
2011/11/17	2.48	5.56	5.56	67.73	20.49	11.22	50.86	13.94	5.61				8.72	2.30	11.66	3.05	1.88									11.66	3.05	3.04	4.84	6.14	
2011/12/8	2.51	5.87	5.87	70.88	20.87	13.24	52.95	14.44		1.36	7.53		8.99		12.07	3.23	1.98									12.07	3.23	3.10	5.83	6.17	
2011/12/29	2.54			76.26	21.25	15.53	57.20	14.64	6.12	2.40	9.88	9.01	9.20	2.56												9.20	3.29	2.01	3.17	6.57	
2012/1/20	2.91	6.79	6.79	88.73	22.08	20.11	60.67	16.18	7.93	2.89	9.94	9.20														9.94	3.87	3.46	7.69		
2012/2/15	3.11	6.89	6.89	87.35	23.29	20.62	3.80	60.80	16.32	8.50	10.12	10.75														10.12	5.27	4.07	8.67		
2012/3/18	3.23	6.90	6.90	91.02	23.75	35.02	7.42	65.22	18.14	8.91	5.30	10.25	12.44													10.25	5.81	4.18	8.62		
2012/4/10	3.25	6.97	6.97	95.20	24.15	37.59	8.21	73.63	21.11	11.88	5.43	11.59														11.59	8.80	4.61	9.18		
2012/5/5	4.49	8.95	8.95	110.05	25.40	40.38	10.71	75.14	22.77	12.56	6.13	12.24														12.24	2.80	4.79	5.91	9.42	
2012/5/21	4.69	6.07	6.07	100.74	26.45	47.66	14.77	77.21	23.75	13.77	6.62	12.25														12.25	13.62	4.92	6.05	9.70	
2012/6/20	4.77	11.10	9.71	104.92	28.52	61.46	21.55	82.67	25.16	14.06	6.98	12.86														12.86	9.09	4.96	6.34		
2012/7/2	5.00	12.10	9.87	105.10	29.12	67.84	24.49	84.60	26.01	14.11	7.75	18.14														18.14	3.58	5.72	6.41	9.83	
2012/7/16	5.40	12.96	11.38	114.92	29.70	74.64	27.84	87.02	27.39	14.88	8.28	18.19														18.19	3.77	6.24	6.47	10.23	
2012/8/10	5.60	17.72	12.31		32.39	82.35	33.76	89.29	28.36	16.07	9.35	18.52														18.52	3.83	4.46	6.38	7.94	11.26
2012/9/3	5.89	16.60	14.10		93.16	37.78	96.42	34.07	18.80	10.62	20.23															20.23	3.94	4.78	7.03	8.44	12.54
2013/4/28		24.95			95.24	48.77		41.07	23.42	16.27	22.62															22.62	4.38	4.50	19.38	5.92	16.57
2013/5/15		23.61	121.15		94.57	48.10		40.43	22.77	15.60	22.04															22.04	4.66	14.83	18.83	5.12	15.52

Table 4 The fitting results of monitoring points

Monitoring point	Coordinates	P_0	P_1	P_2	Correlation coefficient	The initial monitoring time	Current date	Present cumulative monitoring time t/day	Predictive value of the present cumulative settlement (mm)	Predictive rate of the present settlement (mm)	Final predictive value of the cumulative settlement (mm)	Residual value of the settlement (mm)
1	580944.4994	4637443.6049	-0.0174	-52.30	111.01	0.998	2012/7/16	2015/6/25	1074	0.0032	139.30	3.12
2	575884.8325	4637053.0593	-0.0197	-3.66	166.29	0.982	2011/7/19	2015/6/25	1437	0.0001	10.41	0.15
3	576871.0920	4637578.4277	-0.0184	-11.82	280.17	0.984	2011/9/5	2015/6/25	1389	0.0005	34.87	0.58
4	577312.3545	4636929.6982	-0.0083	-15.77	381.11	0.993	2011/9/5	2015/6/25	1389	0.0018	44.69	1.88
5	576885.7268	4637768.4488	-0.0067	-1.21	252.47	0.988	2011/7/19	2015/6/25	1437	0.0001	3.15	0.15
6	576707.9467	4636761.9398	-0.0033	-8.70	54.02	0.988	2011/6/21	2015/6/25	1565	0.0011	15.21	1.72
7	582008.0009	4637133.4287	-0.0042	-64.42	257.33	0.997	2011/2/23	2015/6/25	1583	0.0085	153.93	11.57
8	582644.3634	4637156.2224	-0.0038	-5.09	607.87	0.982	2010/12/28	2015/6/25	1640	0.0012	13.93	1.26
9	583896.7372	4635286.7756	-0.0051	-6.60	395.08	0.996	2010/12/28	2015/6/25	1640	0.0008	17.68	1.03
10	583841.3999	4636509.9367	-0.0056	-1.80	490.36	0.993	2010/12/28	2015/6/25	1640	0.0002	5.03	0.28
11	577599.8017	4637608.0774	-0.0025	-33.51	298.98	0.972	2010/12/28	2015/6/25	1640	0.0068	74.19	9.69
12	578251.8983	4637525.3148	-0.0672	-6.07	225.78	0.999	2010/9/23	2015/6/25	1736	0.0000	18.78	0.16
13	581258.9908	4637810.8767	0.0089	13.63	276.36	0.991	2010/9/23	2015/6/25	1736	0.0007	37.56	1.05
14	576512.8418	4636734.3684	6.2266	15616.00	-441.59	0.977	2010/9/23	2015/6/25	1736	0.0053	56.79	11.51
15	581343.1922	4637539.4402	-0.0070	-18.23	374.75	0.990	2010/9/23	2015/6/25	1736	0.0014	50.59	1.92
16	580532.9267	4637535.7288	-0.0059	-7.24	426.21	0.996	2010/9/23	2015/6/25	1736	0.0007	20.02	0.93
17	579897.3516	4637379.8534	-0.0056	-39.77	245.71	0.998	2010/9/23	2015/6/25	1736	0.0031	100.06	4.72
18	579301.2194	4637304.5680	-0.0031	-110.71	743.54	0.999	2010/9/23	2015/6/25	1736	0.0324	303.08	34.33
19	579289.7009	4637559.9000	-0.0010	-8.83	590.63	0.998	2010/9/23	2015/6/25	1736	0.0038	18.77	6.14
20	578843.5537	4637448.9528	-0.0178	-7.35	638.72	0.988	2010/9/23	2015/6/25	1736	0.0003	22.44	0.38
21	578850.9288	4637607.2832	-0.0025	-20.56	954.56	0.999	2010/9/23	2015/6/25	1736	0.0107	56.40	9.75
22	578277.6379	4637323.7490	-0.0035	-65.03	379.08	0.990	2010/9/23	2015/6/25	1736	0.0095	162.72	13.33
23	578218.6370	4637638.5688	7.6891	529252.00	-975.57	0.978	2010/9/23	2015/6/25	1736	0.0094	70.54	25.37
24	577641.5348	4637123.0744	-0.0118	-35.77	603.34	0.995	2010/9/23	2015/6/25	1736	0.0024	107.38	2.68
25	577624.9408	4637277.7227	-0.0167	-16.87	650.78	0.999	2010/9/23	2015/6/25	1736	0.0009	51.44	0.93
26	577276.0723	4637060.2613	-0.0036	-50.06	415.49	0.985	2010/9/23	2015/6/25	1736	0.0076	127.95	10.30
27	577265.0097	4637203.8633	-0.0015	-34.33	678.63	0.984	2010/9/23	2015/6/25	1736	0.0145	81.47	19.06
28	577233.6655	4637393.4916	-0.0042	-10.70	602.38	0.989	2010/9/23	2015/6/25	1736	0.0019	29.59	2.22
29	577242.8830	4637602.0061	-0.0068	-6.46	666.75	0.994	2010/9/23	2015/6/25	1736	0.0008	18.89	0.89
30	576960.2948	4636996.3966	-0.0043	-10.32	558.29	0.975	2010/9/23	2015/6/25	1736	0.0017	28.38	1.99
31	576923.7630	4637347.4434	-0.0111	-4.46	336.87	0.978	2010/9/23	2015/6/25	1736	0.0002	12.85	0.29
32	576613.2052	4637124.6425	-0.0026	-2.57	401.94	0.994	2010/9/23	2015/6/25	1736	0.0005	6.11	0.72
33	576597.2063	4637318.6278	-0.0163	-5.04	321.63	0.997	2010/9/23	2015/6/25	1736	0.0002	14.87	0.22
34	576170.0000	4637140.0000	-0.0060	-7.94	645.72	0.994	2010/9/23	2015/6/25	1736	0.0011	22.94	1.20
35	576079.1604	4637382.1586	-12.1499	-13200.00	-857.66	0.962	2011/7/19	2015/6/25	1437	0.0021	12.66	4.73
36	579048.9952	4637899.4373	-0.0019	-8.99	861.98	0.992	2010/9/23	2015/6/25	1736	0.0045	23.37	4.82
37	577095.4947	4637760.9342	-0.0006	-19.02	306.65	0.977	2010/9/23	2015/6/25	1736	0.0065	33.15	16.95
38	577969.4484	4637707.6419	-0.0014	-13.96	618.87	0.990	2010/9/23	2015/6/25	1736	0.0057	31.85	7.98

Table 4 continued

Monitoring point	Coordinates	P_0	P_1	P_2	Correlation coefficient	The initial monitoring time	Current date	Present cumulative monitoring time t/day	Predictive value of the present cumulative settlement (mm)	Predictive rate of the present settlement (mm)	Final predictive value of the cumulative settlement (mm)	Residual value of the settlement (mm)
39	581583.9322	4637099.7414	-0.0042	-15.61	380.17	0.984	2011/10/18	1346	36.56	0.0037	40.32	3.76
40	583100.7612	4635238.4845	0.0200	4.68	350.01	0.996	2010/12/9	1659	13.87	0.0001	14.05	0.18
41	582380.1067	4637147.0209	-0.0031	-6.91	-114.65	0.991	2010/12/9	1659	7.26	0.0007	8.52	1.26
42	583863.8234	4635838.6567	-0.0015	-1.63	38.57	0.993	2010/12/9	1659	2.02	0.0004	2.66	0.64
43	583060.6881	4635870.7347	0.1257	0.40	16.42	0.999	2012/8/26	1033	1.08	0.0000	1.08	0.00
44	581617.2207	4635886.7573	-0.0056	-3.89	434.21	0.985	2010/12/9	1659	10.13	0.0005	10.70	0.56
45	581485.7704	4636348.8121	1.5293	10683.70	-383.45	0.982	2012/8/26	1033	13.29	0.0035	18.22	4.93
46	579924.7870	4635952.5753	-0.0706	-4.39	116.50	0.995	2012/5/29	1122	13.21	0.0001	13.27	0.06
47	579934.9271	4635848.4314	-0.0448	-1.10	65.33	0.998	2012/5/29	1122	3.07	0.0000	3.10	0.02
48	579939.2677	4636945.7713	-0.0134	-2.77	61.41	0.989	2012/5/8	1143	6.07	0.0002	6.26	0.19
49	579273.1828	4636812.7615	-0.0035	-62.60	963.35	0.996	2012/12/9	928	72.54	0.2151	178.55	106.01
50	578842.4471	4636833.0015	121.6060	4856060.00	-372.35	0.997	2012/5/8	1143	80.89	0.0174	107.11	26.22
51	578228.1598	4635661.2796	-0.0198	-2.29	623.49	0.996	2012/12/9	928	6.64	0.0012	7.02	0.38
52	578096.3838	4636025.0938	-0.0111	-6.27	462.37	0.998	2012/12/9	928	17.30	0.0025	18.49	1.20
53	577897.7936	4636517.3972	-0.0194	-2.39	75.85	0.988	2012/6/21	1099	5.97	0.0001	6.09	0.12
54	577654.4953	4636892.3025	0.0079	8.52	534.15	0.988	2010/12/9	1659	23.82	0.0008	24.78	0.96
55	576957.6408	4636817.3215	-0.0003	-17.20	728.66	0.938	2011/2/20	1586	7.65	0.0046	30.54	22.89
56	576182.6906	4636781.3306	-0.0343	-1.04	50.51	0.984	2010/12/9	1659	2.69	0.0000	2.93	0.24
57	576455.6387	4635983.1845	-0.0043	-4.94	765.52	0.987	2010/12/9	1659	12.79	0.0014	14.06	1.27
58	576276.5910	4636322.8564	0.0041	10.03	368.74	0.997	2010/12/9	1659	23.76	0.0014	25.64	1.88
59	581546.3404	4636679.2807	-0.0118	-61.46	639.30	0.989	2011/5/8	1509	179.01	0.0068	184.98	5.97
60	577865.7323	4636673.6944	-4.7263	-63392.60	-718.97	0.937	2010/12/9	1659	13.01	0.0024	18.65	5.64



Fig. 4 Images of **a**, **b**, and **c**

is obvious in this area, which is in accordance with the ground survey. At present, the ground subsidence area of the Taihe coal mining is mainly located near the Haixin Road at the south of Tianhu Bridge, as shown in Fig. 4a. The area shows signs of surface collapse and houses submerged in the water. Roadbed subsidence also affects the traffic. As shown in the photo, the height of the road has been adjusted many times, but at present, its height is consistent with that of the wall on both sides of the original road, thus demonstrating subsidence.

Other monitoring points are located outside the scope of the mining areas, mainly in the northwest part of the study area. The area is at the center of the city where the population and their living and working activities are concentrated. This area is still within the scope that is influenced by the main ore mining subsidence deformation, and ground surveys show that there is a wide range of residential buildings with oblique shear fracture caused by ground differential settlement in this area, as shown in Fig. 4b. Therefore, it is necessary to monitor the ground subsidence in this area where important buildings are located. By setting numerous monitoring points to monitor the ground subsidence deformation, the dynamic trends of ground subsidence deformation could be predicted, thus protecting people's lives and properties.

From the overall monitoring data, it could be concluded that the larger ground subsidence deformation area is concentrated in the Laohutai and Taihe mining areas. The final monitoring values of the monitoring points present the trend of gradual decline from the mining spots to the surrounding areas.

The arctangent function prediction model

The origin of the arctangent function prediction model

The arctangent function model is a model of an “S” type curve and was proposed by Nie et al. (2015) through the analysis of surveillance data of monitoring points and the settlement characteristics of the rock mass of different fracture zones in the mined-out area.

$$\delta = p_1 \{ \tan^{-1} p_0(t - p_2) + \tan^{-1} p_0 p_2 \}, \quad (1)$$

where δ is the accumulative settlement value (mm), t is the monitoring time (days); and p_0 , p_1 , p_2 are coefficients that vary with the changes of the monitoring data.

The model parameters are obtained by putting each monitoring value of the single monitoring point and the corresponding cumulative monitoring time into the arctangent function model, and with the help of the Levenberg–Marquardt algorithm (Levenberg 1944; Marquardt 1963; Lourakis 2005), the deformation curve will be obtained. The forecast function will be achieved through obtaining the final settlement deformation values, which will be predicted according to the development trend of the deformation curve.

The model prediction principle

In the arctangent function model, when t tends to be infinite, $\tan^{-1} p_0(t - p_2)$ reaches $\pm\pi/2$, and the curve is close to the asymptote $\delta = p_1 \{ \pm\pi/2 + \tan^{-1} p_0 p_2 \}$. The asymptote value is the final settlement deformation value of the monitoring point. The correlation coefficient is used to evaluate the degree of correlation between the two variables, and the precision of the curve fitting. The correlation coefficient is

$$R = \frac{\sum_{i=1}^n (t_i - \bar{t})(\delta_i - \bar{\delta})}{\sqrt{\sum_{i=1}^n (t_i - \bar{t})^2 \sum_{i=1}^n (\delta_i - \bar{\delta})^2}}. \quad (2)$$

Physical meaning of the model parameters

p_0 represents the speed at which the settlement deformation trend to be stable, the larger the absolute value, the faster. p_2 corresponds to the time (days) of inflection point on the

deformation curve, which represents the cumulative monitoring time of maximum settling velocity. The final predictive value of the cumulative settlement is $p_1(\pm\pi/2 + \tan^{-1} p_0 p_2)$, and when the value of p_0 , p_2 remain unchanged, p_1 will determine the final predictive value of the cumulative settlement.

Applicable scope of the model

It was recognized that surface movements due to underground coal mining activities have three phases: initial, active, and residual subsidence (Tong Liyuan et al. 2015). When a coal face has been fully mined, three main processes occur in the rock and soil mass: crack, caving, and compaction settlement. This progression will be presented as a complete “S” type curve with its deformation characteristics to the surface. If secondary mining activities were done on the coal face, obviously, the characteristics of the original “S” type settlement deformation will be destroyed, and a new development trend of “S” type will generate on the basis of the original deformation characteristics. The accuracy of the prediction model will be greatly reduced once the rock conditions have progressed beyond its applicable scope. Thus, this forecast model is suitable for short- to medium-term predictions under a fully mined area and under constant conditions. The development of mining activities necessitates the constant updating of monitoring data and eliminating previous data that do not conform to deformation characteristics after mining conditions have changed, thereby improving the accuracy of prediction models. This strategy will generate

the appropriate results that are consistent with practical results.

The model feasibility analysis

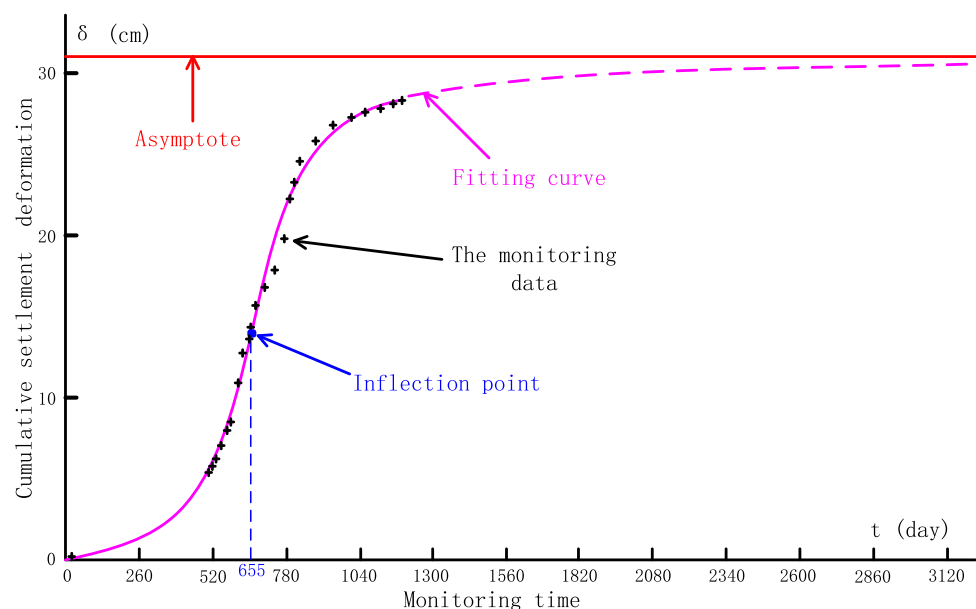
The fitting precision is affected by monitoring errors or changes in the original deformation characteristics of a few stages of ground subsidence caused by external geological forces. However, the “S” type ground subsidence deformation trend, which is caused by underground mining, is not expected to change. Such prediction errors may be mitigated through long-term and effective monitoring and updating of monitoring data, through which the final prediction precision would remain high. Nie et al. (2015) successfully predicted the final settlement deformation value of monitoring point G22 in the Taihe coal mine by applying the arctangent function model. The displacement vs. time fitting curve of monitoring point G22 is shown in Fig. 5. The accuracy of their model is verified by model verification. Thus, in the current study, it is feasible to use the arctangent function model to realize the prediction of ground subsidence.

Model application

Advantages of the prediction model

Ground subsidence prediction research is conducted on the basis of monitoring data. This function model does not require the consideration of interrelations among mining

Fig. 5 Displacement vs. time fitting curve of monitoring point G22 (Nie et al. 2015)



subsidence influencing factors and could overcome the difficulty of obtaining model parameters. Moreover, along with the continuous renewal of monitoring data, the prediction model could repair itself, is simple to operate, could achieve high-precision and dynamic tracking prediction function, and has extensive application. These advantages indicate that the model is appropriate for the current research on mining subsidence and deformation prediction.

Prediction results

In order to obtain the model parameters p_0, p_1, p_2 of every monitoring point, data from the 60 monitoring points in the study area were analyzed by curve fitting with the arctangent function model $\delta = p_1(\pm\pi/2 + \tan^{-1} p_0 p_2)$. Then, the function model of each single point could be achieved by bringing the corresponding model parameters into the forecasting model; this way, the final settlement deformation prediction value of each monitoring point could be obtained. The fitting results of each monitoring point and the final prediction values are shown in Table 4. Due to the different subsidence deformation characteristics of each monitoring point and the different subsidence deformation stage of each point when the monitoring began, huge differences were observed among the parameters p_0, p_1, p_2 .

In this paper, monitoring time of the monitoring points may be irregular, but the whole data could reflect the deformation characteristics and the trends of the monitoring points, and the final fitting precision is very high. Time irregularity in data acquisition will not affect the normal use of the model and the accuracy of prediction.

The monitoring data of the monitoring points were only updated to May 15, 2013, and the current date is June 25, 2015. Residual settlement in Table 4 refers to the rest settlement deformation value from June 25, 2015. To obtain the residual settlement, we first obtained the current cumulative settlement deformation value of the monitoring points. Thereafter, t (i.e., the cumulative monitoring time of each monitoring point corresponding to June 25, 2015) was incorporated to the model to determine the current cumulative settlement deformation value of δ . The settlement deformation rate ν could be obtained based on the model's mathematical properties.

The current settlement deformation rate ν of each monitoring point is predicted by taking the corresponding cumulative monitoring time t into Eq. 3. The residual settlement deformation values and current settlement deformation rate of all monitoring points are shown in Table 4. As can be seen, the 60th monitoring point shows the worst fitting precision with a related coefficient of 0.937, while the other coefficients are all higher than 0.937, and the results of correlation analysis indicate the high precision of the prediction model.

Distribution characteristics of the ground subsidence deformation and the development trend predictions in the study area

Application of Kriging interpolation method

The ground monitoring network is a kind of real-time settlement deformation feedback system and an effective method to study the ground settlement deformation law. However, owing to the terrain conditions, economic conditions, and other factors, a netted, intensive monitoring system cannot be set up in all study areas. In order to study the ground settlement distribution characteristics and its deformation law in the study area, it is necessary to obtain the settlement deformation values of every terrestrial point except the 60 monitoring points in the study area. Kriging interpolation is a method derived from the prediction values of the unknown point by weighting the known sample points; here, a specified mathematical formula is used to decide the output surface smoothness. The Kriging interpolation formula is given by

$$\hat{Z}(s_0) = \sum_{i=1}^N \lambda_i Z(s_i), \quad (3)$$

where $Z(s_i)$ is the measured values of the NO.i location, λ_i is the unknown weight of the measured values of the NO.i location, s_0 is the location for forecasting, and N is the number of known points.

The method reveals the implied trend characteristics of the original data to a maximum extent; it also determines the estimated value under the premise that the estimated value of the research object meets the conditions of unbiasedness and condition of minimum variance. The gridding precision of the Kriging interpolation method is high, the contour produced is relatively smooth, and the drawing effect is good, which are in line with the actual situation field.

Contour maps drawing

The final settlement forecast values, residual settlement forecast values, and the current settlement rate of the 60 monitoring points should be achieved through the model prediction. By using the Kriging interpolation method, the following could be obtained: contour map of the final cumulative settlements of all monitoring points (Fig. 6), contour maps of the residual settlement (Fig. 7), and contour maps of the current settlement rate (Fig. 8). On the one hand, the contour maps obtained the ground subsidence deformation values of all the terrestrial points in the study area by using the method of interpolation. On the other hand, the contour maps could directly reflect the distribution law and deformation characteristics of the ground subsidence in the study area.

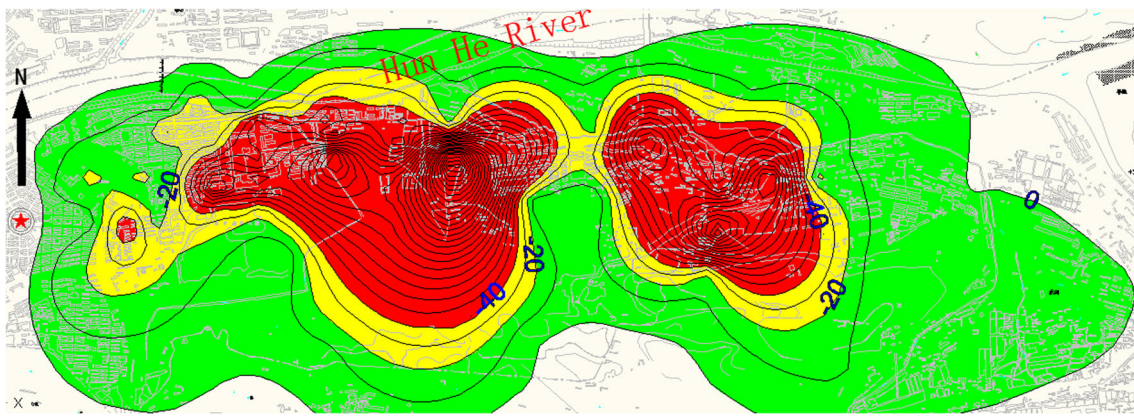


Fig. 6 Contour map of the final cumulative settlement

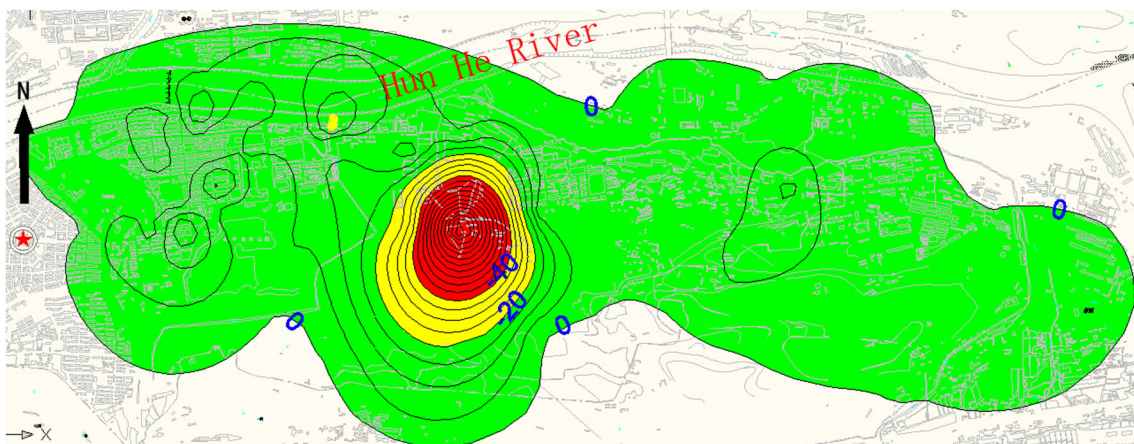


Fig. 7 Contour map of the residual settlement

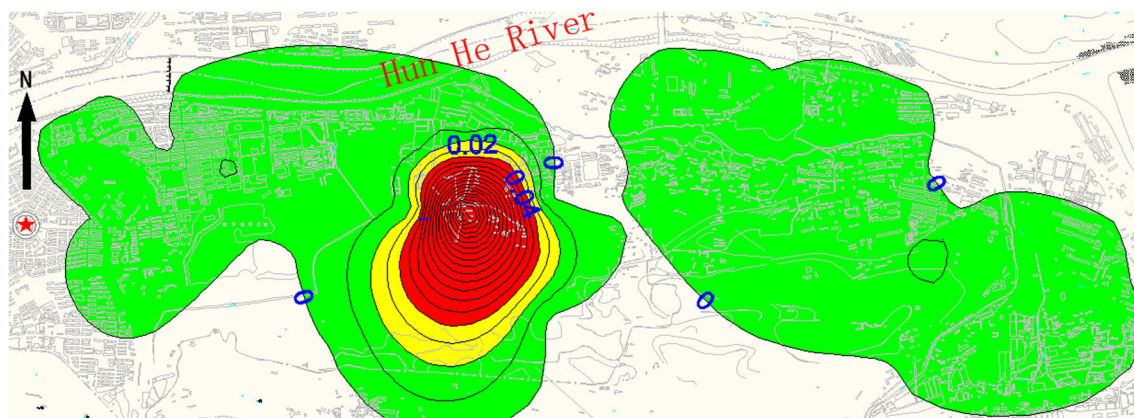


Fig. 8 Contour map of the current settlement rate

Contour map of the final cumulative settlement

Figure 6 shows the contour map of the final cumulative settlement, and directly reflects the distribution law of the total settlement in the study area from the beginning of

monitoring to the settlement stability. Figure 6 also shows that the difference value between the adjacent contour lines is 10 mm. The cumulative settlement deformation value in the red area (6.18 km^2) is larger than 40 mm. The cumulative settlement deformation value in the yellow area

(5.98 km²) is within the range from 20 to 40 mm. Finally, the cumulative settlement deformation value in the red area (15.51 km²) is less than 20 mm.

The slope of surface point i , which is also known as the settlement difference in unit distance, would cause surface building damage when a critical deformation value is obtained, thereby resulting in building dumping, craze, and affecting normal use. In general, the critical deformation value of China is $i = 3.00$ mm/m, whereas the value of those covering a small area but with high structures (e.g., chimneys, water towers, and pylon tower structures) is $i = 1.50$ mm/m. The positions with subsidence deformation values of 40 mm and 20 mm approximately correspond to the surface slopes $i = 3.00$ mm/m and $i = 1.50$ mm/m, respectively. The red areas shown in Fig. 6 denote the unstable ground subsidence area, the yellow areas correspond to the less stable ground subsidence area, and the green areas represent the stable ground subsidence region.

The regions with large final cumulative settlement deformations include the Taihe coal mine, north of the Laohutai coal mine, and northwest of the Longfeng coal mine (Fig. 6). The same figure also shows that the ground subsidence area is generally distributed among the red or yellow areas in accordance with the ground investigation result. Moreover, ground subsidence deformation does not extend to the Hunhe River. Figure 6 presents a gradually decreasing trend of settlement value from the mining spots to the surrounding areas. The density of the settlement isoline represents the surface slope. As the location is considerably near the center of the mining area, the surface slope value increases, the destruction of the buildings is exacerbated, and surface subsidence increasingly develops.

The dependency of the regional subsidence deformation prediction method on monitoring data is relatively high. As some monitoring points within the scope of Taihe coal mining area have been damaged, the effective monitoring points are not enough, especially the lack of data from the key monitoring points, thus it cannot truly show the subsidence deformation characteristics of the area. But from the fitting results and field exploration, the region has tended toward a relatively stable stage, and the prediction results are basically in agreement with the development trend of deformation. But if we want this prediction method to reach its maximum value, it is very important to arrange the key monitoring points in the ground subsidence area.

Contour map of the residual settlement

The contour map of the residual settlement (Fig. 7) is a direct prediction of the rest ground subsidence distribution law from June 25, 2015. Accordingly, the rest settlement difference in unit distance is the evaluation index of the

potential risk of ground subsidence hazards. This parameter can be derived from the contour map of the residual settlement. As shown in Fig. 7, the difference value between the adjacent contour lines is 5 mm. The residual settlement volume in the red area (0.66 km²) is over 40 mm and represents the unstable ground subsidence area in which the surface slope $i > 3.00$ mm/m. The residual settlement volume in the yellow area (0.921 km²) ranges from 20 to 40 mm and represents the less stable ground subsidence area in which the surface slope is expressed as 1.50 mm/m $< i < 3.00$ mm/m. The residual settlement volume in the green area (19.77 km²) is below 20 mm and denotes the stable ground subsidence area with surface slope $i < 1.50$ mm/m.

The red and yellow areas of the large settlement are extensively reduced (Fig. 7) compared with those shown in Fig. 6, and the green area displays the considerable expansion of the stable region. Along with the gradual completion of cumulative ground subsidence, the maximum residual settlement deformation decreased and the danger area gradually stabilized. The Taihe mining area entered a stable ground subsidence stage, but a segment of the surface within the Laohutai mining area retained a large residual settlement, thereby continuing to be a threat to the normal use of buildings. The different settlement characteristics between the two mining areas were mainly caused by the shallow mining depth, as well as a short time for the deformation to reach the surface and for ground subsidence to reach a stable stage in the Taihe coal mine. Therefore, the ground subsidence disaster area would mainly be concentrated in the northeast of the Laohutai mining areas after June 25, 2015 (see red or yellow zones in Fig. 7).

Contour map of the current settlement rate

The current ground settlement rate is the evaluation criterion of the activity of ground subsidence hazards. The contour map of the current settlement rate (Fig. 8) shows that the difference value between the adjacent contour lines is 0.01 mm/d. By combining the ground subsidence deformation monitoring and the current survey results of ground subsidence activities in the field, we divided the ground subsidence activity into strong, medium, and weak stages. These stages correspond to the conditions when the settlement rate of the region satisfied the conditions $v > 0.04$ mm/d, 0.02 mm/d $< v < 0.04$ mm/d, and $v < 0.02$ mm/d, respectively. Hence, the artificially divided activities are relative. The current subsidence rate in the red area (1.26 km²) is over 0.04 mm/d. The current settlement rate in the yellow area (0.89 km²) is within the range of 0.02–0.04 mm/d. The current settlement rate in the green area (16.61 km²) is below 0.02 mm/d. The difference of the current settlement rate in the study area is obvious

(Fig. 8), and the regional distribution characteristics are similar to those of residual settlement deformation. Therefore, the development trend of surface subsidence deformation shows certain regularity.

Risk zoning

Regional assessment is a prediction of the activity and potential risk of ground subsidence hazards in the study area, which could determine the most difficult areas for development and provide the basis for site selection, production safety, and disaster warning (Bell and de Bruyn 1999). The standards of this risk zoning are a combination of the current settlement rate and the rest settlement difference in unit distance. The related details are reflected in Figs. 7 and 8.

Considering the distribution characteristics of the overlapping area of the residual settlement deformation and the current settlement rate, the study area could be divided into five regions (Fig. 9). The overlapping area of the green and green areas is Region I (green part in Fig. 9), which has an area of 19.58 km². Region I represents the area in which the current ground settlement rate is less than 0.02 mm/d, and the ground residual settlement is less than 20 mm. The overlapping area of the green and yellow area is Region II (yellow part in Fig. 9), which has an area of 0.33 km². Region II represents the area in which the current ground settlement rate is within the range of 0.02–0.04 mm/d, and the ground residual settlement is less than 20 mm. Moreover, Region II is the area in which the current ground settlement rate is less than 0.02 mm/d and the ground residual settlement is within the range of 20–40 mm. The overlapping area of the yellow and yellow areas is Region III (orange part in Fig. 9), which has an area of 0.43 km². Region III represents the area in which the current ground settlement rate is within the range of 0.02–0.04 mm/d and

the ground residual settlement is within the range of 20–40 mm. The overlapping area of the yellow and red area is Region IV (magenta part in Fig. 9), which has an area of 0.36 km². Region IV represents the area in which the current ground settlement rate is larger than 0.04 mm/d, and the ground residual settlement is within the range of 20–40 mm. Moreover, in Region IV, the current ground settlement rate is within the range of 0.02–0.04 mm/d, and the ground residual settlement is larger than 40 mm. The overlapping area of the red and red area is Region V (red part in the Fig. 9), which has an area of 0.66 km². Region V represents the area in which the current ground settlement rate is larger than 0.04 mm/d and the ground residual settlement is larger than 40 mm.

In view of the lower current ground settlement rate and rest settlement difference in unit distance in Region I compared to those in the other regions, we conclude that the study area is stable on the basis of ground subsidence. The increase in settlement rate and surface slope from Regions II to V has resulted in the gradual increase in the degree of risk in these regions. Ground residual deformation in these areas may cause continuous damage to surface buildings, underground pipes, aquifers, and even surface subsidence in a few areas. Therefore, monitoring efforts in these areas (i.e., Regions II–V) should be strengthened. Furthermore, the effects of surface subsidence should be considered during production and construction. Finally, corresponding measures should be applied to address ground subsidence disasters and related secondary disasters.

This risk zoning provides a reference for planners and does not directly correspond to the actual risk level but merely a relative risk grading. The construction department may select the appropriate construction area in accordance with its needs, based on the risk-zoning results.

Combined with the assessment of activities and potential risk of ground subsidence geological hazards in the study

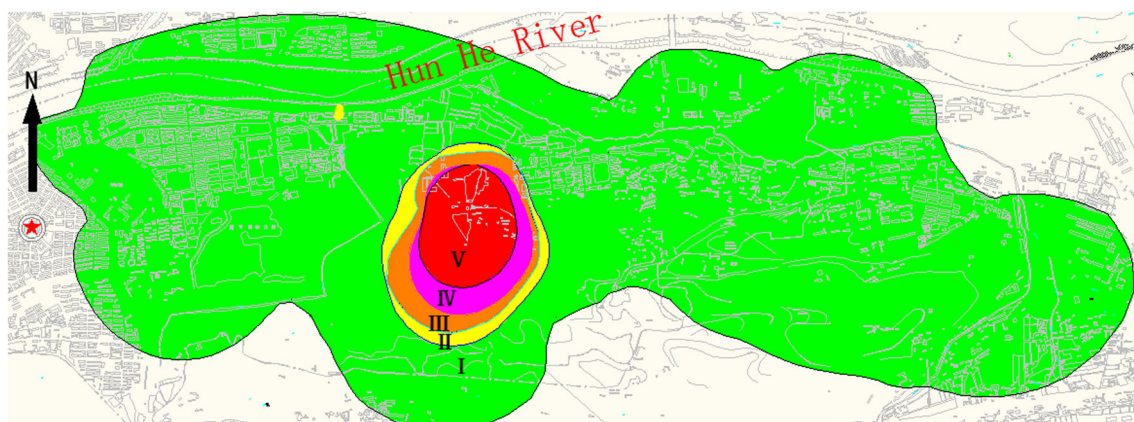


Fig. 9 Risk-zoning map of the ground subsidence in the study area

area, risk zoning could serve as basis for future construction, regional planning, and land utilization in Fushun City. These results could be used to substantially control the occurrence of subsidence accidents, thereby ensuring the safety of people and properties, as well as sustaining economic development in the city.

Conclusions

1. The related coefficients of all 60 monitoring points in the study area are more than 0.937, indicating the high prediction accuracy of the proposed model. The application of the arctangent function model based on monitoring data in the prediction of mining subsidence deformation is, therefore, feasible.
2. Regarding the total settlement deformation distribution in the study area, the regions with a large final cumulative settlement deformation cover the Taihe coal mine, north of the Laohutai coal mine and northwest of the Longfeng coal mine. Hence, the distribution range is extensive. Along with the continuation of ground subsidence, the ground in the Taihe and Longfeng mining areas have basically completed the final settlement deformation. Thus, these areas are considered stable. Ground residual subsidence deformation in the Laohutai coal mine region has also been reduced significantly. Thus, the main settlement deformation zone in the future would be concentrated in the northeast side of the Laohutai mining area near the 49th and 50th monitoring points.
3. Region I (19.58 km²) in the risk-zoning map is the stable ground subsidence area, and the degree of risk from Region II to V (1.78 km²) increases gradually.

Acknowledgments This project was financially supported by the National Natural Science Foundation of China (Grant No. 41172235). Special gratitude is also extended to those participants who have contributed to this work.

References

- Bell FG, de Bruyn IA (1999) Subsidence problems due to abandoned pillar workings in coal seams. *Bull Eng Geol Environ* 57:225–237
- David L, Marschalko M, Yilmaz I, Bednářová P, Niemiec D, Mikulénka V, Kubečka K (2015) Geodetic monitoring of roads as a tool for determination of hazard zones in areas influenced by deep coal mining. *Bull Eng Geol Environ*. doi:10.1007/s10064-015-0769-y
- Díaz-Fernández ME, Álvarez-Fernández MI, Álvarez-Vigil AE (2010) Computation of influence functions for automatic mining subsidence prediction. *Comput Geosci* 14(1):83–103
- Gonzalez-Nicieza C, Alvarez-Fernandez MI, Menendez-Diaz A, Alvarez-Vigil AE (2007) The influence of time on subsidence in the Central Asturian Coalfield. *Bull Eng Geol Environ* 66:319–329. doi:10.1007/s10064-007-0085-2
- Huafeng Xu, Bin Liu, Zhigeng Fang (2014) New grey prediction model and its application in forecasting land subsidence in coal mine. *Nat Hazards* 71(2):1181–1194. doi:10.1007/s11069-013-0656-4
- Nie Lei, Wang Hongfei, Xu Yan, Li Zechuang (2015) A new prediction model for mining subsidence deformation: the arc tangent function model. *Nat Hazards* 75(3):2185–2198. doi:10.1007/s11069-014-1421-z
- Lei Nie, Min Zhang, Heqing Jian (2013) Analysis of surface subsidence mechanism and regularity under the influence of seism and fault. *Nat Hazards* 66:773–780
- Levenberg K (1944) A method for the solution of certain non-linear problems in least squares. *Q Appl Math* 2(2):164–168
- Lourakis MIA (2005) A brief description of the Levenberg–Marquardt algorithm implemented by levmar. *Found Res Technol* 4:1–6
- Marquardt DW (1963) An algorithm for the least-squares estimation of nonlinear parameters. *J Soc Ind Appl Math* 11(2):431–441
- Ruisheng Jia, Yanjun Peng, Hongmei Sun (2011) Mining subsidence prediction based on 3D stratigraphic model and visualization. *Trans Edutainment VI* 6758:206–215
- Sheorey PR, Loui JP, Singh KB, Singh SK (2000) Ground subsidence observations and a modified influence function method for complete subsidence prediction. *Int J Rock Mech Min Sci* 37:801–818
- Tong L, Leo L, Amatya B, Liu S (2015) Risk assessment and remediation strategies for highway construction in abandoned coal mine region: lessons learned from Xuzhou. *Bull Eng Geol Environ, China*. doi:10.1007/s10064-015-0760-7
- Wanghua Sui, Yuan Hang, Ma Luxing Wu, Zhaoyang Zhou Yongjie, Guoqing Long, Lianbo Wei (2015) Interactions of overburden failure zones due to multiple-seam mining using longwall caving. *Bull Eng Geol Environ* 74(3):1019–1035
- Ximin Cui, Jiachen Wang, Yisheng Liu (2001) Prediction of progressive surface subsidence above longwall coal mining using a time function. *Int J Rock Mech Min Sci* 38:1057–1063
- Ximin Cui, Li Chunyi Hu, Qingfeng Miao Xiexing (2013) Prediction of surface subsidence due to underground mining based on the zenith angle. *Int J Rock Mech Min Sci* 60:246–252
- Zhang B, Zhang L, Yang H, Zhang Z, Tao J (2015) Subsidence prediction and susceptibility zonation for collapse above goaf with thick alluvial cover: a case study of the Yongcheng coalfield Henan Province China. *Bull Eng Geol Environ*. doi:10.1007/s10064-015-0834-6
- Zhanqiang Chang, Jinzhuang Wang, Mi Chen, Ao Zurui, Qi Yao (2015) A novel ground surface subsidence prediction model for sub-critical mining in the geological condition of a thick alluvium layer. *Front Earth Sci* 9(2):330–341